

Supporting Information

Enhancing light hydrocarbons storage and separation through introducing Lewis basic nitrogen sites within a carboxylate-decorated copper-organic framework

Xiuping Liu, Weidong Fan, Minghui Zhang, Guixia Li, Haijun Liu, Daofeng Sun, Lianming Zhao*, Houyu Zhu, Wenyue Guo*

College of Science, China University of Petroleum, Qingdao, Shandong 266580, People's Republic of China.

E-mail: lmzhao@upc.edu.cn; wyguo@upc.edu.cn.

Tel: +86-532-8698-3363; Fax: +86-532-8698-3363.

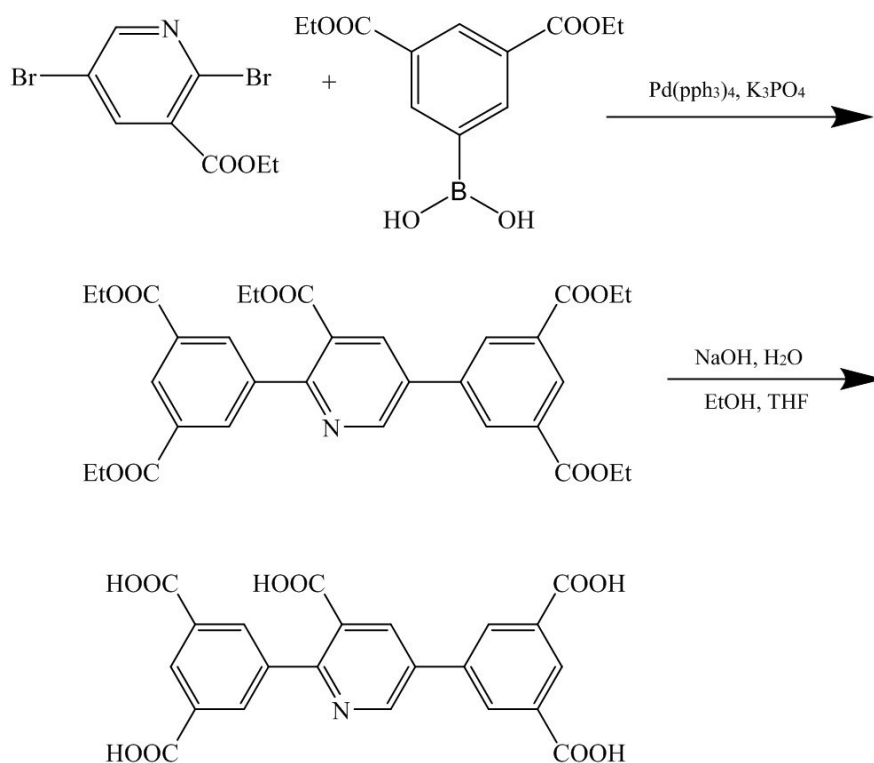
Table of contents

1. Materials and Methods.....	3
1.1 Synthesis of materials.....	3
1.2 Crystal data of NEM-4.....	6
1.3 Determination of single-crystal structure.....	7
1.4 A typical procedure for the dye adsorption experiments.....	8
1.5 Computational methods.....	9
1.6 Calculation of Selectivity.....	12
2. The linker central ring orientations in 1 and NEM-4.....	14
3. Powder X-ray diffraction of NEM-4.....	15
4. IR spectra of NEM-4.....	16
5. The TG curve of NEM-4.....	17
6. The gas adsorption in NEM-4.....	18
7. GCMC and first-principles calculations for NEM-4.....	22
8. The dye adsorption in NEM-4.....	25

1. Materials and Methods

1.1 Synthesis of materials

(a) Ligand H₅N



Scheme S1. Synthetic route of H₅N.

The ligand H₅N (2,5-bis(3',5'-dicarboxyphenyl)-benzoic acid) was synthesized analogous to the procedure described in the literature.¹ Generally, a Suzuki-coupling reaction of 2,5-dibromo-3-pyridinecarboxylic acid ethyl ester and 3,5-diethylisophthalate-5-boronic acid was involved (Scheme S1). 2,5-dibromo-3-pyridinecarboxylic acid ethyl ester (3.09 g, 10 mmol), 3,5-dicarboxyethylester-phenylboronic acid (5.853 g, 22 mmol), K₃PO₄ (20.0 g, 95 mmol), and dioxane (300 ml) were combined in a 500 ml three-necked flask and stirred in an oil bath equipped with a magnetic stirrer. The mixture was bubbled with argon for 30 min and then

degassed on the Schlenk line and refilled with argon. Pd(PPh₃)₄ (500 mg, 0.43 mmol) and dioxane (300 ml) were introduced into the flask under an argon atmosphere and heated with stirring at 90 °C for 72 hours, and then the mixture was filtered and washed with chloroform for three times at ambient temperature. The resulting gray oil was then dissolved with few amount of chloroform and was purified by silica gel column. After removing the organic solvents, white solid of carboxylate ester was obtained (yield: 3.23 g, 51.6 %) and hydrolyzed with NaOH (12 g, 300 mmol) in THF/EtOH/H₂O (2/2/3, 250 ml) solution and finally acidified with concentrated HCl to afford the white precipitate (named as H₅N, 1.07 g, 45.26 %), which was confirmed by the ¹H NMR spectrum (Figure S1).

(b) Complex NEM-4

A mixture of Cu(NO₃)₂·3H₂O (24 mg, 0.1 mmol) and H₅N (10 mg) was dissolved in 4 ml DMA/EtOH/H₂O mixed solvent (v/v/v = 2/1/1), and then 0.1 ml HBF₄ was added. All the reagents were sealed in a glass bottle and slowly heated to 85°C from room temperature in 6 h. After keeping at 85°C for 50 h, the mixture was slowly cooled to 30°C at a rate of 7°C/h. The pale-blue block crystals could be collected after washed with DMA and dried in the air. The sample of NEM-4 in 72.6% yield based on copper was insoluble in common solvent, such as H₂O, dichloromethane, methanol, DMSO, or DMF.

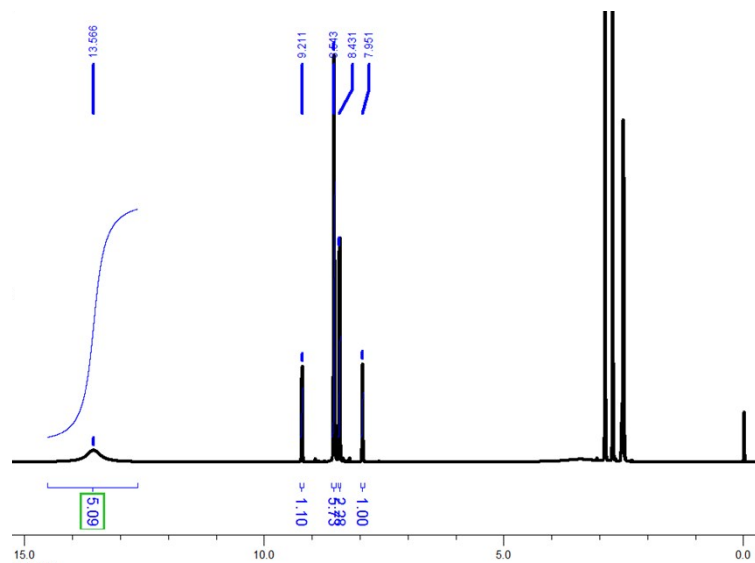


Fig. S1 ^1H NMR spectrum of H_5N in $\text{d}_6\text{-DMSO}$.

1.2 Crystal data of complex NEM-4

Table S1 Crystal data and structure refinement for complex NEM-4

Parameters of crystal structure	Values
Formula	C ₄₈ Cu ₂ O ₂₁ H ₅₉ N ₅
M	1169
Crystal system	Trigonal
Space group	<i>R-3m</i>
<i>a</i> /Å	18.5961(2)
<i>b</i> /Å	18.5961(2)
<i>c</i> /Å	38.2100(7)
α /deg	90.0
β /deg	90.0
γ /deg	120.0
V/Å ³	11443.3(3)
Z	36
GOF	1.050
R ₁ ^a /wR ₂ ^b I > 2σ(I)	0.0703,0.2073
R ₁ , wR ₂ (all data)	0.0640,0.2003
R _{int}	0.0189

$$^a R_1 = \frac{\sum ||F_o| - |F_c||}{\sum |F_o|}, \quad ^b wR_2 = [\frac{\sum w(F_o^2 - F_c^2)^2}{\sum w(F_o^2)^2}]^{0.5}.$$

1.3 Determination of single-crystal structure

Single crystal of the prepared complex with appropriate dimensions was chosen under an optical microscope and quickly coated with high vacuum grease (Dow Corning Corporation) before being mounted on a glass fiber for data collection. Data for NEM-4 were collected on Super Nova diffractometer equipped with a Cu-K α radiation X-ray sources ($\lambda = 0.71073 \text{ \AA}$) and an Eos CCD detector under 100 K. For NEM-4, data were measured using scans of 0.5° per frame for 10 s until a complete hemisphere had been collected. Data reduction was performed with the CrysAlisPro package, and an analytical absorption correction was performed. The structures were treated anisotropically, whereas the aromatic and hydroxy-hydrogen atoms were placed in calculated ideal positions and refined as riding on their respective carbon or oxygen atoms. Structure was examined using the Addsym subroutine of PLATON² to assure that no additional symmetry could be applied to the model.

1.4 A typical procedure for the dye adsorption experiments

Before adsorption, NEM-4 was dried overnight under vacuum at 100°C and kept in a desiccator. In the adsorption process, the adsorbent (5 mg) was weighed precisely and immersed in CH₃OH solutions (5 ml) containing dye molecules (concentration: 4×10⁻⁵ mol l⁻¹), such as methylene blue (MB⁺), crystal violet (CV⁺), rhodamine B (RB⁺), methyl orange (MO⁻), and Sudan II (SD⁰). Then the UV-Vis spectra of CH₃OH solutions containing both dyes and adsorbent were measured at 25°C at different time points (10 min to 12 h) to calculate the dye concentrations by comparing the UV-Vis absorbance of the dye and adsorbent containing solutions at various time to that of the original dye containing solution.

To obtain the adsorption capacity, NEM-4 (10 mg) was immersed in 10 mL of MB⁺ solutions with a known dye concentration between 50 and 200 ppm. 12 hours later, the solution was separated from the adsorbent with a syringe filter and UV-Vis was used to analyze the residual concentrations of MB⁺. The equilibrium adsorption capacity Q was calculated according to Eq.

$$Q = \frac{(C_0 - C)V}{m} \quad (1)$$

The C₀ and C (mg L⁻¹) were the initial and final concentrations of MB⁺, respectively.

V (L) was the volume of the solution, and m (g) was the mass of sorbent.

1.5 Computational methods

Density functional theory (DFT) calculations: DFT calculations were performed to provide the atomic partial charges on the NEM-4 framework for the grand canonical Monte Carlo (GCMC) calculations as well as to give the optimized structures and energies of C₂H₂, C₂H₄, C₂H₆, C₃H₆, C₃H₈, CO₂, and CH₄ interaction with the fragmented cluster of NEM-4. We used the Perdew–Burke–Ernzerhof (PBE) functional under the generalized gradient approximation (GGA) functional with the double- ξ numerical polarization (DNP) basis set implemented in the DMol³ program package in the Materials Studio of Accelrys Inc for our calculations. Since calculations using the whole unit cells are too expensive, we used fragmented cluster models cleaved from the unit cells for modeling the partial charges, structures, and energies, the cleaved bonds at the boundaries of the clusters were saturated with protons (hydrogens) (see Figures 5, S9, and S11). The tolerances of energy, gradient and displacement convergence were 1×10^{-5} hartree, 2×10^{-3} hartree \AA^{-1} , and 5×10^{-3} \AA , respectively. The atomic charges in complex NEM-4 (Table S4) were estimated by fitting to the electrostatic potential (ESP) obtained with the CHELPG method,³ which has been successfully used to describe the behavior of other MOFs.⁴ The adsorption energies (ΔE_{ad}) of gas molecules with the fragmented cluster were calculated by $\Delta E_{\text{ad}} = E_{\text{gas-cluster}} - E_{\text{gas}} - E_{\text{cluster}}$, where E_{gas} , E_{cluster} , and $E_{\text{gas-cluster}}$ are the total energies of the gas molecule, the fragmented cluster, and the adsorption system at their optimized geometries, respectively.

Grand canonical Monte Carlo (GCMC) calculations: In this work, the adsorption isotherm of pure C_2H_2 adsorption in NEM-4 was simulated using the grand canonical Monte Carlo (GCMC) method implemented in the MUSIC code. Periodic boundary conditions were applied in three dimensions. A combination of site-site Lennard-Jones (LJ) and Coulombic potentials was used to calculate the gas-gas and gas-framework interactions. The site-site LJ potential was described by the LJ (12, 6) model, and the electrostatic interaction was calculated via the Coulomb law. All the interaction parameters conform to Lorentz-Berthelot mixing rules, i.e., $\epsilon_{ij} = (\epsilon_{ii}\epsilon_{jj})^{1/2}$, $\sigma_{ij} = (\sigma_{ii} + \sigma_{jj})/2$.⁵ During the simulations, the framework was rigid considering the negligible influence of framework flexibility on the adsorption of gas under the low-energy conditions.⁶ The linear acetylene molecule is a rigid structure where the C-C and C-H bond lengths are fixed at 1.2111 and 1.0712 Å, respectively. To represent the van der Waals interactions, the acetylene molecule was treated as a two-site model, in which H atoms in acetylene molecule were represented as non-interacting atoms. The LJ parameters and partial atomic charges of C_2H_2 molecule were taken from Fischer,⁷ which have shown excellent results for C_2H_2 storage in MOF materials.⁸ The atomic partial charges of the NEM-4 framework were taken from our DFT results (Table S4), and were adjusted slightly to make the whole system maintain charge neutrality. The LJ parameters for NEM-4 atoms were taken from ref. 9. The cutoff distance for truncation of the intermolecular (LJ) interactions was set to 8 Å, and the Ewald sum technique was used to compute the electrostatic interaction. The number of trial

moves was 2×10^7 . The first 10^7 moves were used for equilibration, and the subsequent 10^7 moves were performed to sample the desired properties.

1.6 Calculation of Selectivity

Myers and Prausnitz developed Ideal Adsorption Solution Theory (IAST) to estimate the amount adsorbed of each component of a mixture using the isotherms for the single components.¹⁰ The theory assumes that the adsorbed gases form an ideal solution, and therefore the method is applicable at relatively low pressures and surface coverages. It uses spreading pressure to characterize the adsorbed phase and assumes that the adsorbent structure is thermodynamically inert with its surface area being independent of the adsorbate. The isotherms of the pure components are fitted to appropriate equations to provide a mathematical description of the isotherm and fitted by the single-site Langmuir-Freundlich equation.

The equation for the calculation of selectivity (S) between gas 1 and gas 2 is shown as

$$S = \frac{x_1/y_1}{x_2/y_2} \quad (2)$$

where x_i and y_i are the mole fractions of component i in the adsorbed and gas phase, respectively, and i equals 1 or 2. In this work, selectivities for equimolar binary gases of CO_2/CH_4 , $\text{C}_2\text{H}_2/\text{CH}_4$, $\text{C}_2\text{H}_4/\text{CH}_4$, $\text{C}_2\text{H}_6/\text{CH}_4$, $\text{C}_3\text{H}_6/\text{CH}_4$, $\text{C}_3\text{H}_8/\text{CH}_4$ have been calculated for NEM-4 at ambient conditions (i.e., 295 K and up to 1 bar).

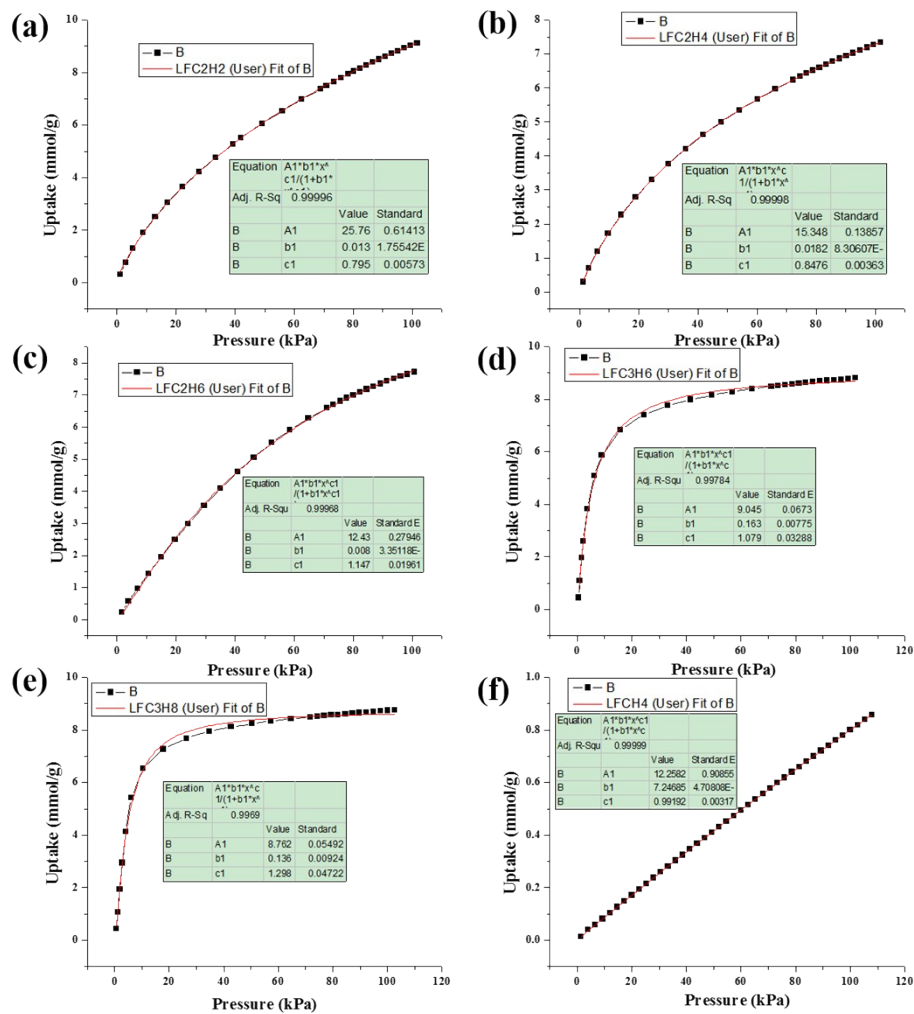


Fig. S2 IAST fitting of the (a) C_2H_2 , (b) C_2H_4 , (c) C_2H_6 , (d) C_3H_6 , (e) C_3H_8 adsorption isotherms for NEM-4.

2. The linker central ring orientations in **1** and NEM-4

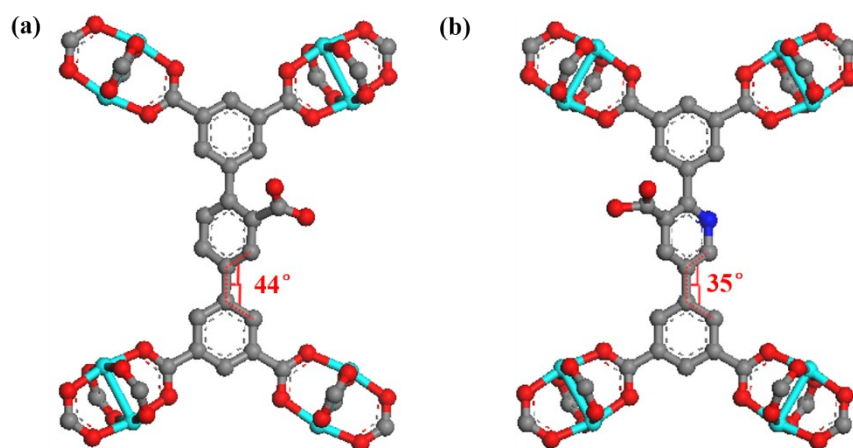


Fig. S3 Illustration of dihedral angle between the two coplanar end benzene rings and central ring in the linker of (a) **1** and (b) NEM-4.

3. Powder X-ray diffraction of NEM-4

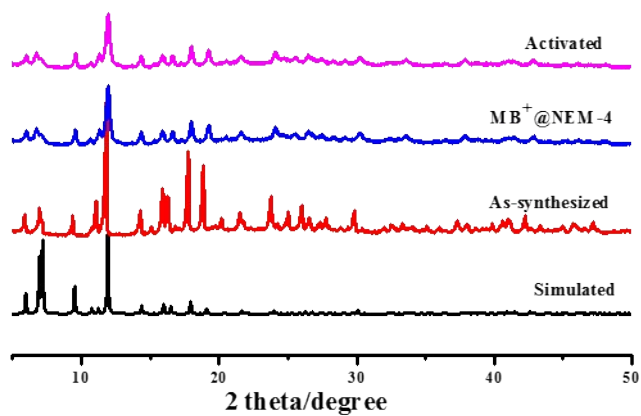


Fig. S4 XRD patterns of NEM-4 simulated from X-ray crystal diffraction data (black) and measured for NEM-4 samples in the as-synthesized (red), MB^+ adsorbed (blue), and activated (magenta) states, respectively.

4. The TG curve of NEM-4

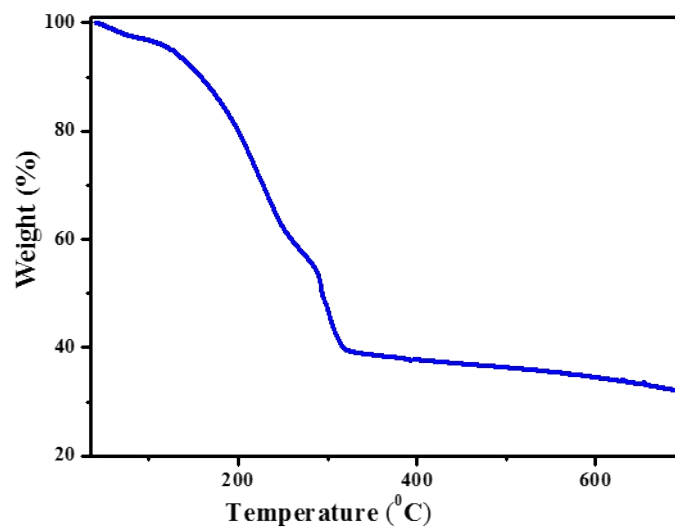


Fig. S5 TG curve of NEM-4.

5. IR spectra of NEM-4

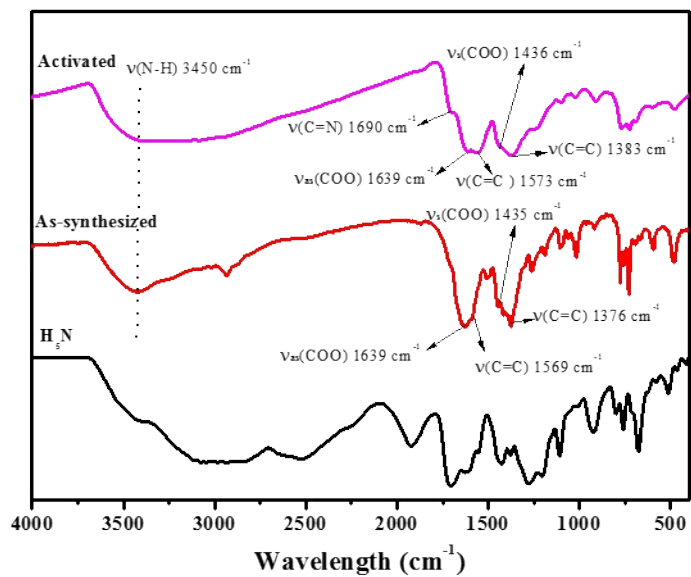


Fig. S6 FT-IR spectra of ligand H₅N and NEM-4 in the as-synthesized and activated states.

6. The gas adsorption in NEM-4

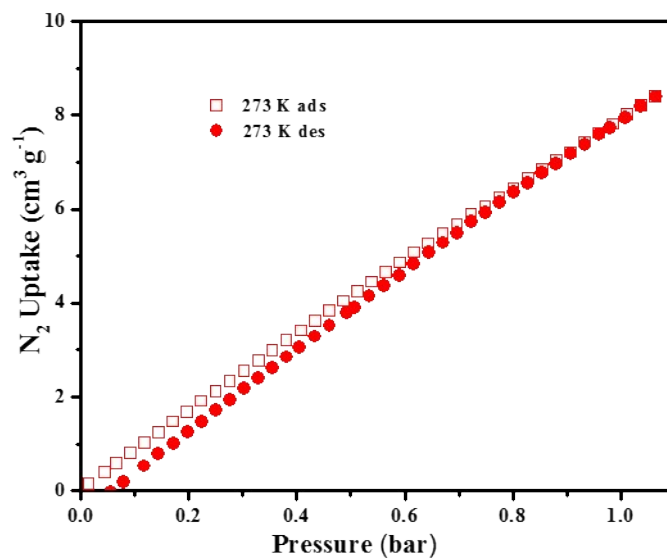


Fig. S7 N₂ adsorption isotherm at 273 K of complex NEM-4.

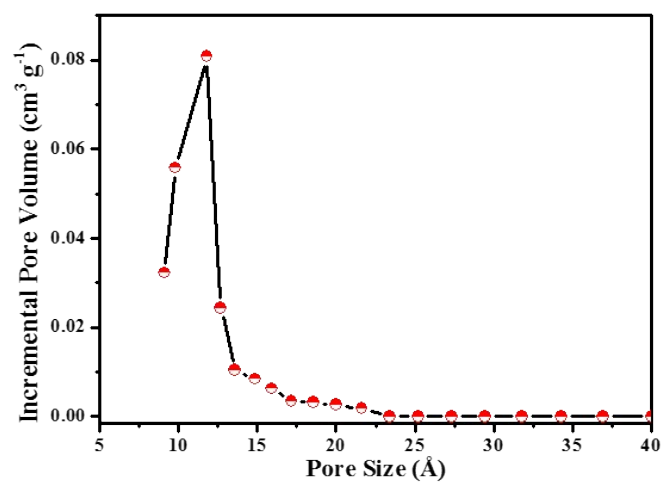


Fig. S8 Pore size distribution for NEM-4 evaluated by using N₂ adsorption data measured at 77 K.

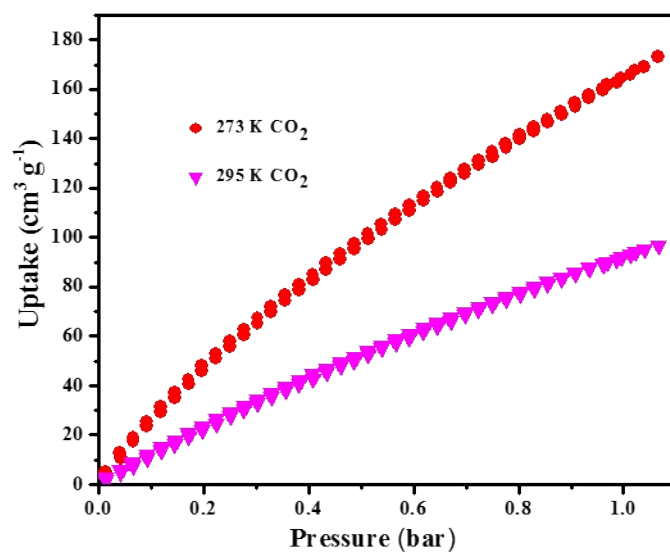


Fig. S9 CO₂ adsorption isotherm at 273 K and 298 K for NEM-4.

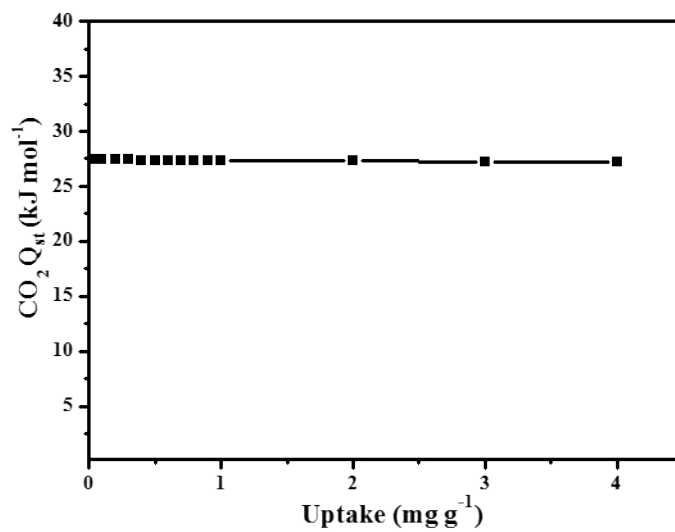


Fig. S10 The Q_{st} of CO₂.

Table S2 Comparison of light hydrocarbons uptakes (in cm³ g⁻¹) in a series of MOFs

MOFs	CH ₄	C ₂ H ₂	C ₂ H ₄	C ₂ H ₆	C ₃ H ₆	C ₃ H ₈	Ref.
NEM-4 ^a	19.3	204	164.1	172.2	197.4	196.1	This work
1^a	17.6	190	147.1	156.6	170	173	36
MFM-202a ^b	10.1	77.1	64.9	94.3	160.8	151.4	38
Cu-TDPAT ^c	28.2	177.6	164.4	154.3			39
MFM-300 ^b	6.5	142	95.9	19.04			38
UPC-21 ^a	25.7	140	98.4	104.3	110	103	44
Fe ₂ (dobdc) ^d	17.2	154.3	134.8	112	149.2	127	43
PAF-40 ^d	12.1		40.3	43.7		53.5	38
PAF-40-Fe ^d	13.9		51.7	41.4		57.8	38
ZJU-11 ^c	22	165	157	154			12
UTSA-35a ^e	9.6	65	48.4	54.4	73.7	66.5	42

^a at 295 K and 1 bar. ^b at 293 K and 1 bar. ^c at 298 K and 1 bar. ^d at 318 K and 1 bar. ^e at 296 K and 1 bar.

7. GCMC and first-principles calculations for NEM-4

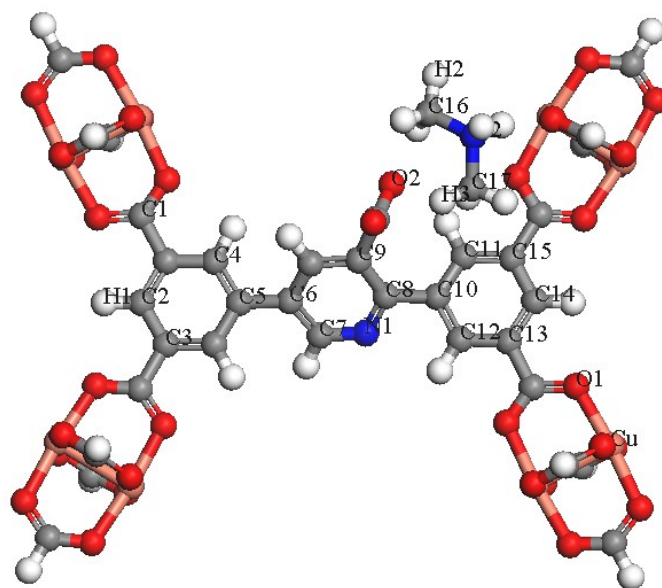


Fig. S11 Atomic representations of the fragmented cluster model of complex NEM-4.

Table S3 Partial charges (in e) of atoms in the fragmented cluster model of NEM-4

Atom	Charge	Atom	Charge	Atom	Charge
O1	-0.573	C7	0.236	C15	0.053
O2	-0.560	C8	0.636	C16	-0.445
C1	0.654	C9	-0.443	C17	-0.485
C2	-0.20	C10	-0.1	N1	-0.568
C3	0.022	C11	-0.118	N2	0.141
C4	-0.169	C12	-0.201	H1	0.180
C5	0.089	C13	0.087	H2	0.159
C6	-0.155	C14	-0.252	H3	0.212
Cu	0.965				

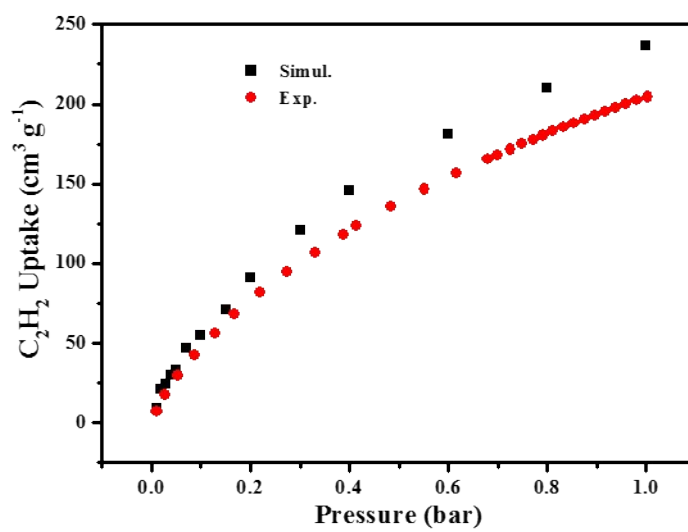


Fig. S12 The simulated and experimental excess adsorption isotherm of C₂H₂ in NEM-4 at 273 K.

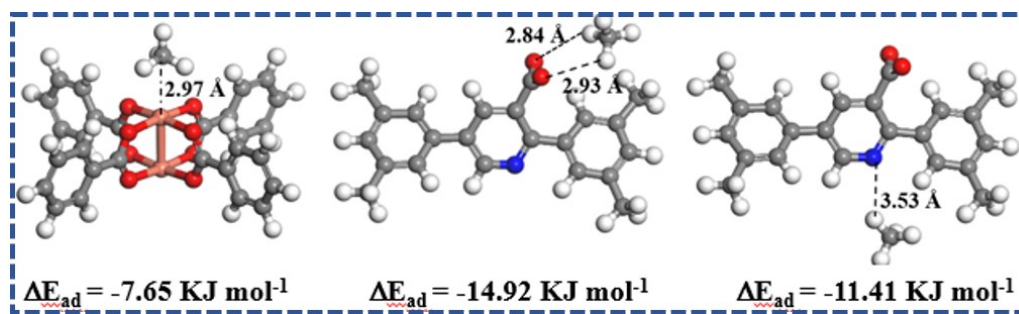


Fig. S13 Preferential CH₄ adsorption sites and corresponding binding energies in NEM-4 obtained from first-principles calculations.

8. The dye adsorption in NEM-4

Ionic MOFs may have more unique advantages such as selective adsorption of cationic/anionic dyes by host-guest electrostatic interactions and/or guest-guest exchange interactions [57]. In this section, we first investigated the charge of the NEM-4 and determined the uptakes of dye molecules with different charged states (Fig. S14), i.e., MB^+ , Sudan II (SD^0), and methyl orange (MO^-) in their methanol solutions (5 ml, 4×10^{-5} M). After the NEM-4 samples were put into the corresponding solutions, the concentration of the cationic MB^+ is drastically decreased (Fig. 7a), whereas both the neutral SD^0 and anionic MO^- dyes show only a slight decline in concentration after 12 h (Fig. S15c,d). Correspondingly, the color of MB^+ solution fades away obviously, whereas it retains for the SD^0 and MO^- solutions even after 12 h (Fig. S16). The separation performance of NEM-4 for the 1:1 MB^+/MO^- and MB^+/SD^0 mixtures in methanol solutions was further explored. As shown in Fig. 7c,d, NEM-4 could only selectively absorb MB^+ , and the solutions almost show the colors of pure SD^0 or MO^- at last (Fig. S17c,d). Moreover, the MB^+ molecules loaded in NEM-4 (Fig. 7b) can be released quickly and efficiently in the NaCl-containing methanol solutions; the release efficiency is up to 62.1% after 150 min. However, in the pure methanol solution only a trace amount of MB^+ can be released. These facts indicate that the release of dyes is triggered by the ion-exchange process occurred between MB^+ in NEM-4 and Na^+ in the NaCl-containing methanol solution.

The influence of dye molecular size on its ability to be absorbed by NEM-4 was also studied. All three organic dyes MB⁺, crystal violet (CV⁺), and rhodamine B (RB⁺) are positively charged, but with different molecular sizes following MB⁺ < CV⁺ < RB⁺ (Fig. S14 and Table S4). In contrast to the good adsorption performance for MB⁺ as mentioned above, NEM-4 is indeed unable to adsorb RB⁺ or weakly captures CV⁺ from the methanol solution, mirrored by the variation of the dye concentrations induced by NEM-4 (Fig. S15a,b). The maximum MB⁺ adsorption capacity of NEM-4 was estimated to be 685 mg g⁻¹ by adding 10 mg as-synthesized NEM-4 into 10 ml of dye CH₃OH solution at room temperature for 12 h (Fig. S18), which is higher than structural analogues NOTT-101 (400 mg g⁻¹) but lower than ZJU-24 (902 mg g⁻¹).²⁸ Then, NEM-4 was put into the 1:1 mixed MB⁺/RB⁺ and MB⁺/CV⁺ methanol solutions. The UV-Vis spectra indicate that the peak corresponding to MB⁺ decreases quickly with time, whereas it decreases relatively slowly for CV⁺ or does not change for RB⁺ even after 12 h (Fig. 7e,f). Correspondingly, the color of the mixed MB⁺/RB⁺ and MB⁺/CV⁺ solutions tends to be close to the color of the pure RB⁺ and CV⁺ solutions after 12 h (Fig. S17a,b), respectively. All these facts suggest that molecular size is an important factor for dye to be captured by NEM-4.

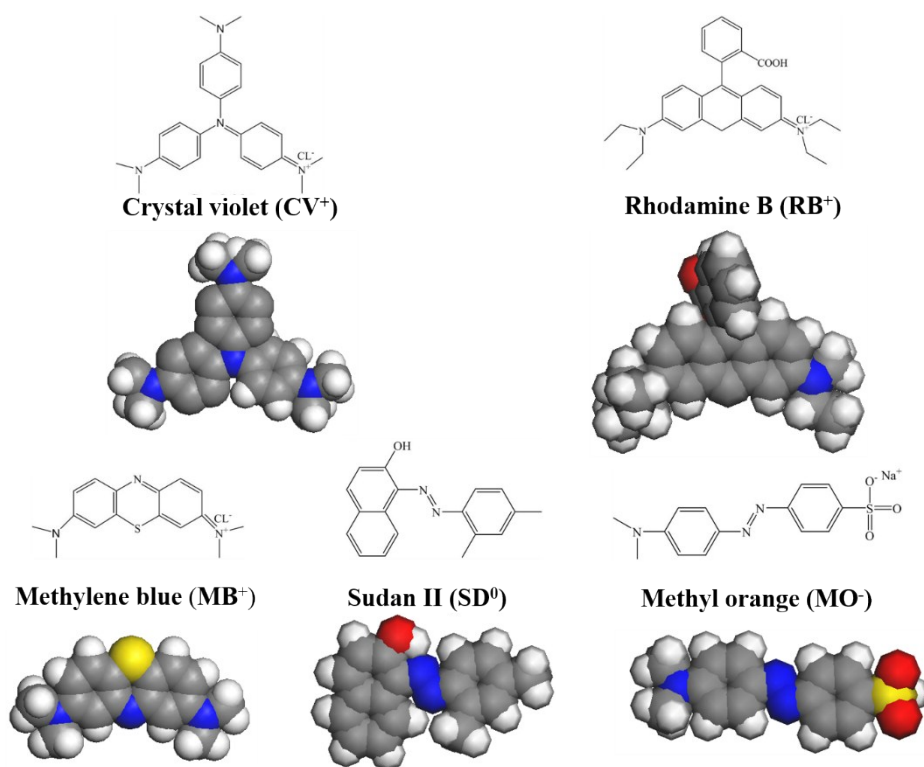


Fig. S14 The structural formula of the studied dye molecules.

Table S4 Molecular dimensions of dye molecules with different charges

	MB ⁺	CV ⁺	RB ⁺	SD ⁰	MO ⁻
a (Å)	2.62	4.78	6.53	3.88	4.14
b (Å)	5.94	12.42	11.89	7.21	5.65
c (Å)	14.61	13.10	15.55	11.06	13.65

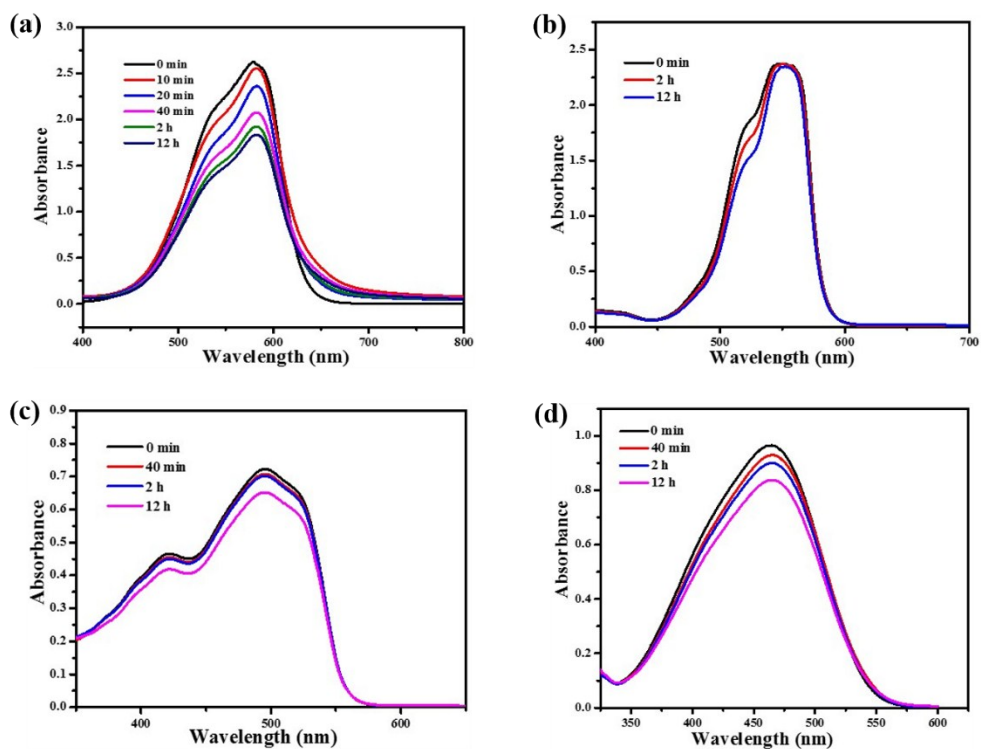


Fig. S15 UV-Vis spectra of the CH₃OH solutions containing (a) CV⁺, (b) RB⁺, (c) SD⁰, and (d) MO⁻ at different time points in an adsorption test with NEM-4.

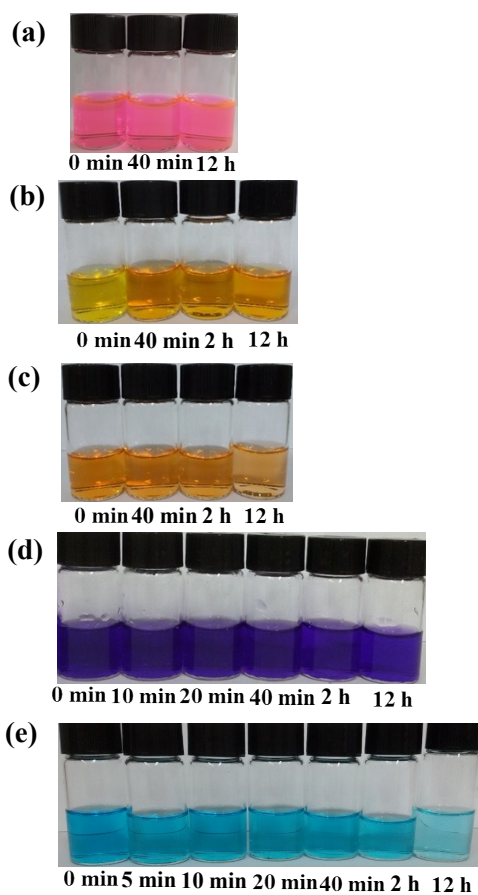


Fig. S16 Photographs of the CH₃OH solutions containing (a) RB⁺, (b) SD⁰, (c) MO⁻, (d) CV⁺ (d), and (e) MB⁺ at different time points in an adsorption test with NEM-4.

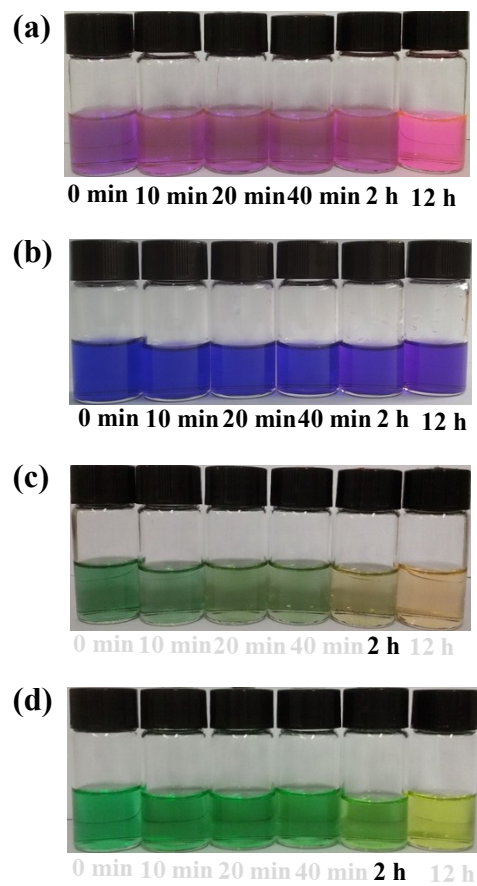


Fig. S17 Photographs of the CH₃OH solutions containing (a) MB⁺/RB⁺ (1:1), (b) MB⁺/CV⁺ (1:1), (c) MB⁺/SD⁰ (1:1), and (d) MB⁺/MO⁻ (1:1) dye mixtures at different time points in an adsorption test with NEM-4.

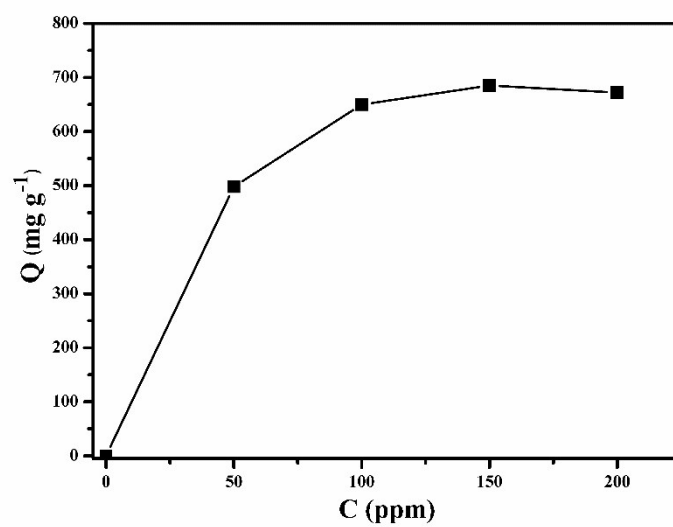


Fig. S18 Adsorption isotherms for MB⁺ adsorption in NEM-4, C: equilibrium concentration of adsorbate, Q: the amount of adsorbate adsorbed.

References

- 1 L. G. Li, J. G. Bell, S. F. Tang, X. X. Lv, C. Wang, Y. L. Xing, X. B. Zhao, K. M. Thomas, *Chem. Mater.*, 2014, 26, 4679–4695.
- 2 S. Ding, X. Sun, Y. Zhu, Q. Chen, Y. Xu, *Crystallogr* 2006, 62, i269–i271.
- 3 U. C. Singh, A. P. Kollman, *J. Comput. Chem.*, 1984, 5, 129–145.
- 4 R. Babarao, J. Jiang, *Energy Environ. Sci.*, 2009, 2, 1088–1093.
- 5 A. A. Clifford, P. Gray, N. Platts, *J. Am. Chem. Soc.*, 1977, 73, 381–382.
- 6 Q. Yang, D. Liu, C. Zhong, R. J. Li, *Chem. Rev.*, 2013, 113, 8261–8323.
- 7 M. Fischer, F. Hoffmann, M. Froba, *Chem. Phys. Chem.*, 2010, 11, 2220–2229.
- 8 M. X. Zhang, B. Li, Y. Z. Li, Q. Wang, W. Zhang, B. Chen, S. Li, Y. Pan, X. You, J. Bai, *Chem. Commun.*, 2016, 52, 7241–7244.
- 9 O. Y. Yang, C. L. Zhong, *Chem. Phys. Chem.*, 2006, 7, 1417–1421.
- 10 A. L. Myers, J. M. Prausnitz, *AIChE J.*, 1965, 11, 121–127.
- 11 X. Duan, H. Wang, Z. Ji, Y. Cui, Y. Yang, *J. Solid State Chem.*, 2016, 241, 152–156.
- 12 X. Duan, H. Wang, Z. Ji, Y. Cui, Y. Yang, G. Qian, *Mater. Lett.*, 2017, 196, 112–114.